Antenna Decoupling by Common and Differential Modes Cancellation

Libin Sun, *Graduate Student Member, IEEE*, Yue Li, *Senior Member, IEEE*, Zhijun Zhang, *Fellow, IEEE*, and Hanyang Wang, *Senior Member, IEEE*

***Abstract*— In this article, a general decoupling method based on a new perspective of common mode (CM) and differential mode (DM) cancellation is proposed. For two closely spaced antennas, the mutual coupling effect can be analyzed and solved by exciting them simultaneously with in-phase (CM) and out-of-phase (DM) signals. It is theoretically proved that, if CM and DM impedances are the same, the mutual coupling effect between two separated antennas can be totally eliminated. Therefore, we can solve the coupling problem by CM and DM impedance analysis and exploit the unique field properties of characteristic modes to assist in antenna decoupling in a physical intuitive way. To validate the feasibility of this method, two practical design examples, including the decoupling between closely spaced dipole antennas and planar inverted-F antennas, are proposed. Both design examples have demonstrated that the proposed method can provide a systemic design guideline for antenna decoupling and achieve better decoupling performance compared to the conventional decoupling techniques. We forecast the proposed decoupling scheme, with a simplified decoupling procedure, has great potential for the applications of antenna arrays and multi-input multi-output (MIMO) systems.**

***Index Terms*— Antenna decoupling, common mode (CM), differential mode (DM), mode cancellation, multi-input multi-output (MIMO), mutual coupling.**

I. Introduction

MUTUAL coupling effect between antenna elements is an intrinsic issue of antenna array or multi-input multi-output (MIMO) antenna system, which will significantly degrade the antenna efficiency and affect the diversity performance [1]–[4]. To tackle this issue, plenty of decoupling methods and techniques have been investigated to eliminate the mutual coupling effect in antenna arrays. Specifically, orthogonal mode method employs the orthogonal nature of physical quantities, such as polarizations [5]–[10], radiation patterns [11], [12], and phases [13], [14] to design decoupled MIMO antennas with a natural high isolation. However, it is hard to solve the coupling problem between closely spaced antenna elements with the same physical property by the orthogonal mode method. Accordingly, a serious of decoupling techniques are presented to suppress the mutual coupling effect between nearby elements in antenna arrays. Electromagnetic band gap (EBG) [15]–[17] and detected ground structures (DGS) [18]–[23], both possess band-stop response, can suppress the surface-wave coupling effect between antenna elements. Neutralization line (NL) [24]–[28] and parasitic elements [29]–[37] can provide a new coupling path with equal amplitude but out-of-phase to achieve the coupling cancellation. Recently, a novel decoupling metasurface [38]–[41] is proposed to solve the mutual coupling problem in large-scale antenna arrays by the out-of-phase cancellation of coupled waves and reflected waves. However, in the above decoupling techniques, the characteristic modes of antenna elements are not effectively exploited to assist in antenna decoupling, which will make the decoupling process really complicated and time-consuming. The coupler technology [42]–[44] can provide a route to realize common mode (CM) and differential mode (DM) for two symmetrical antenna elements. However, the coupler should be finely modified to address the impedance mismatching issue caused by the strong mutual coupling between antenna elements [43], [44]. Therefore, the complex and bulky feed network and asymmetric radiation properties limit the application scenarios of this technology.

In this article, we propose a simple and efficient decoupling method based on a new perspective of CM and DM cancellation [45]. In our method, decoupling between two symmetrical antenna elements is theoretically equivalent to the impedance matching of CM and DM. Then, the unique field properties of CM and DM can be exploited to assist in comprehending the coupling issue and eliminating the mutual coupling effect by adjusting CM and DM impedances independently. When we obtain the same impedance status for CM and DM, the coupling current in the passive antenna element can be canceled out absolutely by the superposition of CM and DM. To validate the feasibility of this method, two practical design examples, including the mutual coupling reduction between closely spaced electric-type antennas (dipoles) and magnetic-type antennas [planar inverted-F antennas (PIFAs)], are proposed. Both design examples have demonstrated that the proposed methodology could offer a systemic design guideline, simplified decoupling procedure, and satisfactory decoupling performance.

This article is organized as follows. In Section II, the decoupling methodology of CM and DM cancellation is presented. In Section III, the design example of dipole antennas

Manuscript received January 2, 2020; revised June 6, 2020; accepted July 2, 2020. Date of publication July 21, 2020; date of current version February 3, 2021. This work was supported by the National Natural Science Foundation of China under Contract 61971254 and Contract 61525104. *(Corresponding author: Zhijun Zhang.)*

Libin Sun, Yue Li, and Zhijun Zhang are with the Beijing National Research Center for Information Science and Technology (BNRist), Tsinghua University, Beijing 100084, China (e-mail: zjzh@tsinghua.edu.cn).

Hanyang Wang is with Huawei Technology Ltd., Berkshire RG2 6UF, U.K. (e-mail: hanyang.wang@huawei.com).

Color versions of one or more of the figures in this article are available online at https://ieeexplore.ieee.org.

Digital Object Identifier 10.1109/TAP.2020.3009427

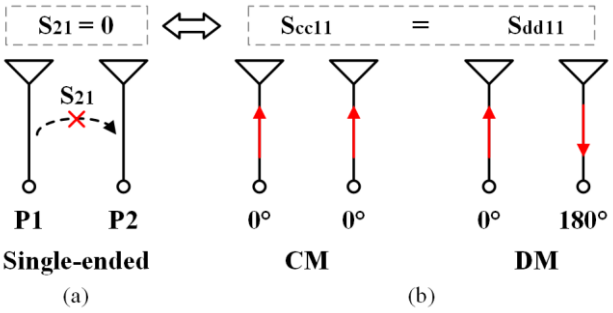

Fig. 1. Decoupling conditions for an arbitrary dual-antenna system from two different perspectives. (a) Single-ended model and corresponding decoupling condition. (b) CM and DM models and corresponding decoupling condition.

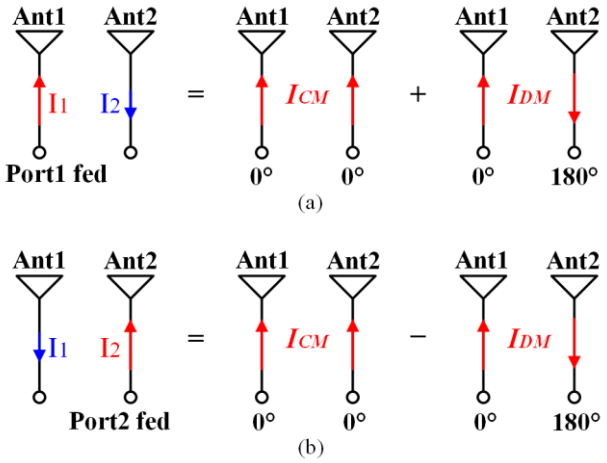

Fig. 2. Relationships of current distributions. (a) Port1 is driven and port2 is loaded with 50 Ω. (b) Port2 is driven and port1 is loaded with 50 Ω.

decoupling is reported with detailed design guideline, antenna performance, and comparison. In Section IV, the design example of PIFAs decoupling is reported with detailed design guideline, antenna performance, and comparison. Finally, Section V draws a conclusion of this article.

II. Principle of CM and DM Cancellation

A. S-Parameters Analysis

Shown in Fig. 1(a) is the sketch diagram of an arbitrary two-port antenna system. As we all know, the aim of antenna decoupling is to let $S_{21} = 0$ from the perspective of single-ended S-parameters. Alternatively, as shown in Fig. 1(b), we can also regard the two-port antenna system as a whole and analyze it from the perspective of mixed mode (CM and DM) S-parameters. The CM and DM S-parameters are [46]

$$S_{cc11} = (S_{11} + S_{12} + S_{21} + S_{22})/2 \quad (1)$$

$$S_{dd11} = (S_{11} - S_{12} - S_{21} + S_{22})/2. \quad (2)$$

Specifically, a symmetrical and reciprocal 2-port network satisfies the conditions of $S_{11} = S_{22}$ and $S_{12} = S_{21}$. Therefore, the CM and DM S-parameters for a symmetrical and reciprocal two-port antenna system can be simplified to

$$S_{cc11} = S_{11} + S_{21} \quad (3)$$

$$S_{dd11} = S_{11} - S_{21}. \quad (4)$$

Combined with (3) and (4), we have

$$S_{21} = S_{12} = (S_{cc11} - S_{dd11})/2 \quad (5)$$

$$S_{11} = S_{22} = (S_{cc11} + S_{dd11})/2. \quad (6)$$

In terms of (5), we can conclude that the decoupling equation of $S_{21} = 0$ can be equivalent to $S_{cc11} = S_{dd11}$ when we consider the decoupling issue from the perspective of CM/DM system. That is, for an arbitrary symmetrical and reciprocal two-port antenna system, if CM and DM S-parameters are the same, the mutual coupling effect between two separated antennas can be totally eliminated. This conclusion could offer a new insight into antenna decoupling, which will be analyzed in detail in Sections III and IV.

B. Current Analysis

To have an intuitive view of the decoupling principle from the perspective of the CM/DM system, the relationships of current distributions are reported in Fig. 2. When port1 is driven and port2 is loaded with 50 Ω, Ant1 is excited with current I_1 with a strong coupled current I_2 on Ant2. Due to the orthogonal nature of CM and DM, the CM current $\boldsymbol{i_{CM}} = [I_0, I_0]^{\mathrm{T}}$ and DM current $\boldsymbol{i_{DM}} = [I_0, -I_0]^{\mathrm{T}}$ could be regarded as a set of basis current of the two-port antenna system. Accordingly, the currents I_1 and I_2 can be expressed as the linear addition of basis currents $\boldsymbol{i_{CM}}$ and $\boldsymbol{i_{DM}}$ as shown in Fig. 2(a), and it can be deduced as

$$\boldsymbol{I_{P1}} = \begin{bmatrix} I_1 \\ I_2 \end{bmatrix} = \boldsymbol{I_{CM}} + \mathbf{I_{DM}} = \alpha \boldsymbol{i_{CM}} + \beta \boldsymbol{i_{DM}} = \frac{1 - S_{cc11}}{2}\begin{bmatrix} I_0 \\ I_0 \end{bmatrix} + \frac{1 - S_{dd11}}{2}\begin{bmatrix} I_0 \\ -I_0 \end{bmatrix} \quad (7)$$

where α and β are the complex excitation coefficients of CM and DM basis currents, respectively, which are related to the S-parameters of CM and DM.

When port2 is driven and port1 is loaded with 50 Ω, Ant2 is excited with current I_2 with a strong coupled current I_1 on Ant1. Symmetrically, as shown in Fig. 2(b), currents I_1 and I_2 can be expressed as the linear subtraction of $\boldsymbol{i_{CM}}$ and $\boldsymbol{i_{DM}}$, and it can be deduced as

$$\boldsymbol{I_{P2}} = \begin{bmatrix} I_1 \\ I_2 \end{bmatrix} = \boldsymbol{I_{CM}} - \mathbf{I_{DM}} = \alpha \boldsymbol{i_{CM}} - \beta \boldsymbol{i_{DM}} = \frac{1 - S_{cc11}}{2}\begin{bmatrix} I_0 \\ I_0 \end{bmatrix} - \frac{1 - S_{dd11}}{2}\begin{bmatrix} I_0 \\ -I_0 \end{bmatrix}. \quad (8)$$

According to (7), Table I summarizes some typical states with different values of CM and DM S-parameters. As seen, if CM and DM have the same S-parameter, the coupling current in the passive antenna element I_2 can be canceled out absolutely with a perfect isolation, whereas the difference in CM and DM S-parameters will lead to the incomplete current cancellation. Therefore, the key to antenna decoupling is to

TABLE I
SOME TYPICAL STATES WHEN FED THROUGH PORT1

S_{cc11}	S_{dd11}	I_1	I_2	S_{21}	Status
0	0	I_0	0	0 (-∞ dB)	Isolated
0	1	$I_0/2$	$I_0/2$	-1 (0 dB)	Full coupled
1	0	$I_0/2$	$-I_0/2$	1 (0 dB)	Full coupled
C_0	C_0	$(1-C_0)\ I_0$	0	0 (-∞ dB)	Isolated
C_1	C_2	$(1-C_1/2-C_2/2)\ I_0$	$(C_2/2-C_1/2)\ I_0$	$(C_1-C_2)/2$	Partially coupled

*C_0, C_1, C_2 are complex numbers.

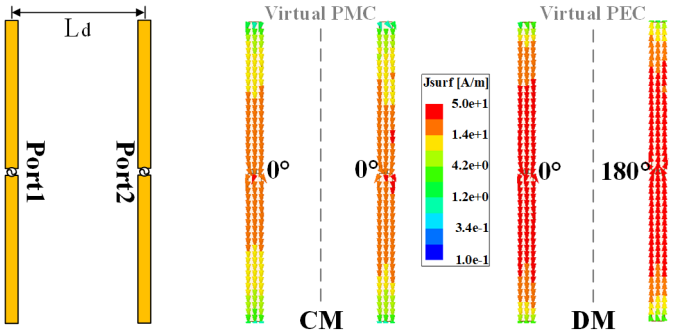

Fig. 3. Model of two closely spaced dipoles separated by a distance of 0.2 λ_0 and the corresponding current distributions by CM and DM excitations.

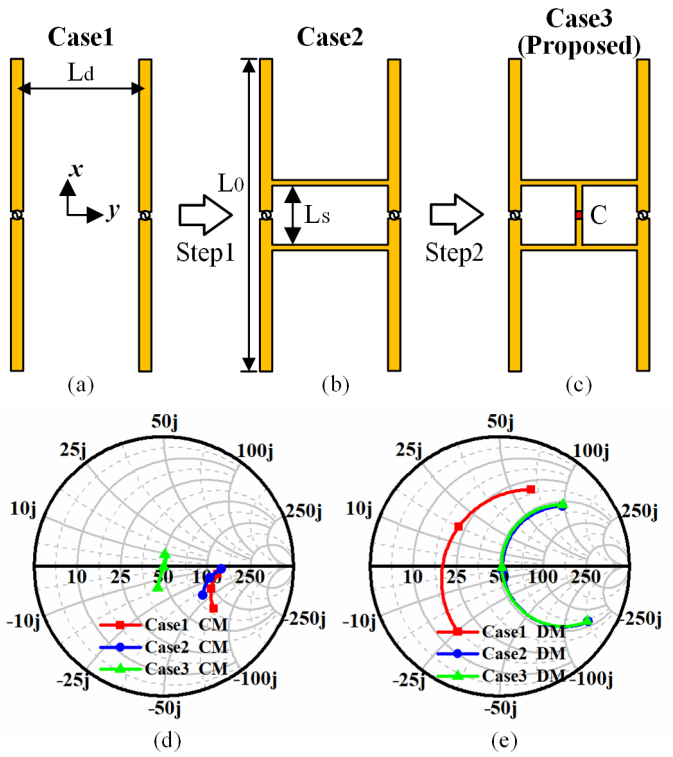

Fig. 4. Evolution procedure of dipole decoupling and corresponding Smith charts of CM and DM. Detailed dimensions: $L_d = 40$ mm, $L_0 = 96.5$ mm, Ls = 17 mm, and C = 0.25 pF. (a) Case1: closely spaced dipoles separated by 0.2 λ_0. (b) Case2: two horizontal strips are added in-between. (c) Case3 (proposed): a vertical strip and lumped capacitance are added between two horizontal strips. (d) Smith charts of CM impedance. (e) Smith charts of DM impedance.

keep CM and DM impedances in the same state for achieving a perfect current cancellation in the passive element.

III. DESIGN EXAMPLE OF DIPOLE ANTENNAS

To demonstrate the feasibility and features of the proposed CM and DM cancellation method, a design example of decoupling between two closely spaced dipole antennas is proposed in this section. As we all know, decoupling between closely spaced dipole antennas is a classic problem. And parasitic scatter [29], [30] is the well-known approach for the dipole antennas decoupling, however, it suffers from a narrow bandwidth. Here, based on the CM and DM cancellation method, we propose a simple and efficient structure to decouple between closely spaced dipoles with an enhanced bandwidth performance.

A. Design Guideline

Fig. 3 shows two $\lambda/2$ resonant dipole antennas separated by a distance L_d of 40 mm (0.2 λ_0). To analyze the coupling problem from the perspective of CM and DM, the corresponding current distributions with in-phase and out-of-phase excitations are illustrated in Fig. 3. When fed with in-phase signals, common currents are driven on two dipoles and the center plane can be equivalent to a virtual PMC plane. On the contrary, when fed with out-of-phase signals, differential currents are driven on two dipoles and the center plane can be equivalent to a virtual PEC plane. As seen, the excited current strength of DM is higher than CM, which leads to the incomplete current cancellation in the passive element as analyzed in Section II-B. Consequently, we should tune CM and DM impedances to the same state for matching the current strengths of CM and DM.

The evolution procedure of the dipole antenna decoupling as well as the corresponding Smith charts of CM and DM impedances in the evolution procedure are proposed in Fig. 4. As shown in Fig. 4(d) and (e) (red line), in Case1, the CM impedance is much higher than 50 Ω while the DM impedance is much lower than 50 Ω. The impedance discrepancy between CM and DM leads to the strong coupling between two dipoles. Although many approaches can realize the impedance tuning of CM and DM, the interaction between CM and DM impedances makes the tuning process very complicated. Accordingly, it is crucial to find a way to adjust CM and DM impedances independently. Fortunately, the unique field properties of CM and DM make the independent impedance tuning possible, which can be summarized as the following two steps.

Step1: Insert two symmetrical horizontal strips between dipole antennas as shown in Fig. 4(b). Due to the center PMC boundary condition for CM, the horizontal strips cannot excite effective current in CM as shown in Fig. 5(a). On the contrary, as shown in Fig. 5(b), the center PEC boundary condition for DM can support a strong current distribution in the horizontal

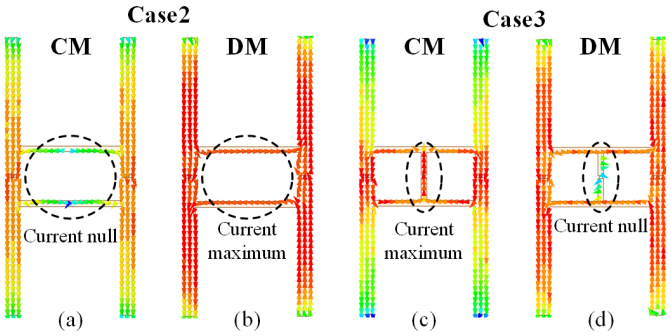

Fig. 5. Simulated current distributions in (a) Case2 with CM excitation, (b) Case2 with DM excitation, (c) Case3 with CM excitation, and (d) Case3 with DM excitation.

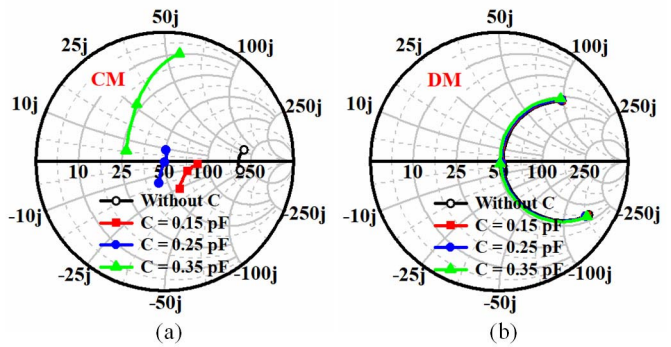

Fig. 6. Smith charts of (a) CM and (b) DM impedances with the variation of inserted capacitance C.

strips for DM. Consequently, the horizontal strips can adjust DM impedance independently while CM impedance keeps unchanged as shown in Fig. 4(d) and (e) (blue line). Specifically, *Ls* is a key parameter for DM impedance matching and a good DM impedance matching is achieved when $Ls = 17$ mm.

Step2: Insert a vertical strip and a lumped capacitance between two horizontal strips as shown in Fig. 4(c). For CM, the center PMC boundary condition can support a strong current distribution in the vertical strip, as shown in Fig. 5(c). On the contrary, as shown in Fig. 5(d), the center PEC boundary condition for DM cannot support effective current in the vertical strip. Therefore, the vertical strip can adjust CM impedance independently while DM impedance keeps unchanged as shown in Fig. 4(d) and (e) (green line). However, the vertical strip cannot make a sufficient impact on the CM impedance, hence a lumped capacitance is inserted in-between for further adjustment. Fig. 6 shows the influence of the inserted capacitance on CM and DM impedances. As shown in Fig. 6(a), the CM impedance can hardly match to 50 Ω when without the capacitance. With the variation of capacitance, the CM impedance is sharply altered and it achieves an optimized matching status when C = 0.25 pF. On the contrary, the DM impedance is not affected by the capacitance C, as shown in Fig. 6(b), due to the center virtual PEC boundary.

B. Decoupling Performance

After the above two steps, both CM and DM impedances are in the same matching status. Accordingly, the mutual coupling between port1 and port2 can be canceled out according to (5). The single-ended S-parameter in the evolution procedure is shown in Fig. 7. As seen, the original isolation between two dipole antennas is only 7.5 dB. After inserting the proposed decoupling structure, the isolation is obviously improved to better than 40 dB at 1.5 GHz as well as a satisfactory decoupling bandwidth. Meanwhile, S_{11} bandwidth almost keeps unchanged with the insertion of the proposed decoupling structure.

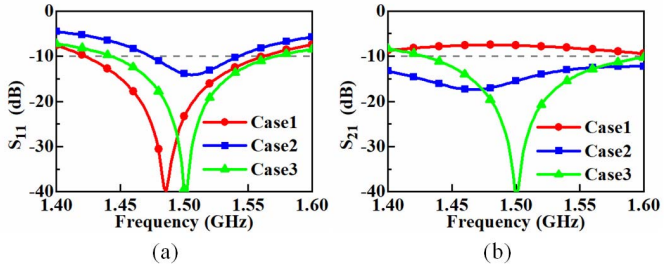

Fig. 7. Simulated (a) S_{11} and (b) S_{21} in Case1, Case2, and Case3.

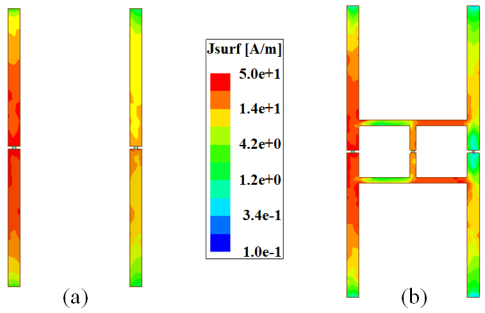

Fig. 8. Simulated current distributions (a) without and (b) with the decoupling structure when fed through port1.

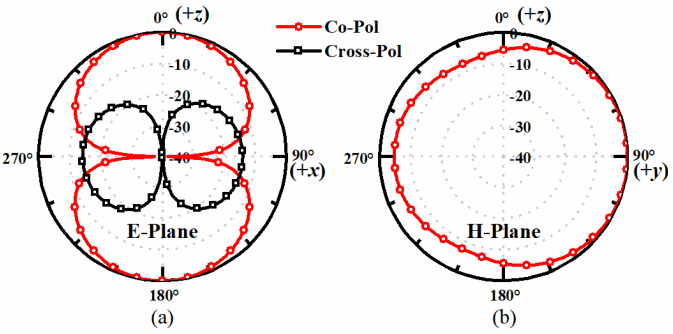

Fig. 9. Simulated radiation pattern of the proposed decoupled dipole antennas at 1.5 GHz when fed through port1. (a) E-plane. (b) H-plane.

To physically demonstrate the decoupling performance, the current distributions without and with the decoupling structure is proposed in Fig. 8. If without the decoupling structure, two dipoles are strongly coupled due to the radiated wave effect. After inserting the proposed decoupling structure, the coupled current in port2 is totally canceled out owing to the complete cancellation of CM and DM currents.

TABLE II
COMPARISON OF THE DECOUPLING PERFORMANCE BETWEEN CLOSELY SPACED DIPOLE ANTENNAS

Ref	Distance	Bandwidth*	Peak Isolation
[29]	0.16λ	~2.0%	14 dB
[30]	0.1λ	0.66%	> 40 dB
Proposed	0.2 λ	8.7%	41.4 dB
	0.1 λ	3.3%	29.4 dB
	0.075 λ	1.5%	16.2 dB

* Overlapping bandwidth of S_{11} < -10 dB and S_{21} < -10 dB.

The radiation pattern of the proposed decoupled dipole antennas when fed through port1 is presented in Fig. 9. As seen, an "8"-shaped copolarized radiation pattern is formed with a cross-polarization level of −14 dB in E-plane. The omnidirectional radiation in H-plane is slightly affected due to the influence of inserted strips and passive element, which leads to a gain variation of 4.7 dBi in H-plane.

To highlight the merits of our decoupling scheme, the decoupling performance of closely spaced dipole antennas is compared in Table II. In addition, the proposed decoupling scheme is also suitable when the element distance is smaller, such as 0.1 λ and 0.075 λ, the optimized results of which are also included in Table II. As seen, our decoupling scheme possesses much better bandwidth performance than the conventional decoupling technique [29], [30]. Moreover, in our scheme, the unique field properties of characteristic modes are effectively analyzed and exploited to assist in designing the decoupling structure instead of performing complex network analysis.

IV. DESIGN EXAMPLE OF PIFA ANTENNAS

The decoupling performance of closely spaced electric-type antennas (dipoles) is demonstrated in Section III. In this section, the decoupling performance of closely spaced magnetic-type antennas (PIFAs) is proposed to validate the universality of the proposed CM and DM cancellation method.

A. Design Guideline

Fig. 10(a) shows two strongly coupled PIFAs with a side-by-side distance of d = 2 mm (0.01 λ_0). The PIFAs are modeled in the air medium with a profile of 8 mm (0.04 λ_0). The two PIFAs are directly fed by metal probes at port1 and port2, respectively. The E-field distributions of CM and DM are illustrated in Fig. 10(b) and (c), respectively. With the in-phase excitation, the common E-field distribution is excited in two PIFAs, which enables y-direction equivalent magnetic currents. On the contrary, with the out-of-phase excitation, a differential E-field is excited in two PIFAs, which cancels the y-direction equivalent magnetic currents. However, the center and fringe radiation apertures can be effectively excited, which enables an x-direction equivalent magnetic currents as shown in Fig. 10(c). Therefore, CM radiates an x-polarized field while DM radiates a y-polarized field.

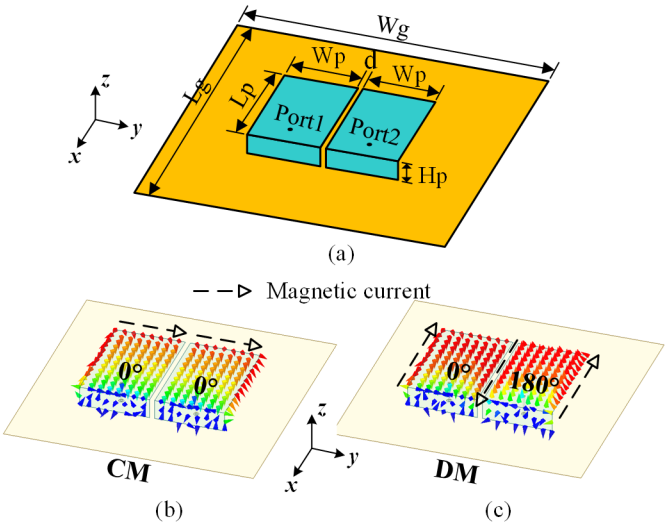

Fig. 10. (a) Model of two extremely closely spaced PIFAs with a side-by-side distance d = 0.01 λ_0. (b) Vector E-field distribution of CM with in-phase excitation. (c) Vector E-field distribution of DM with out-of-phase excitation.

For the PIFA structure, there are many parameters to tune the CM and DM impedance matching and bandwidth. For CM, the impedance matching and bandwidth can be tuned by the size of the ground plane, i.e., W_g and L_g [47]. For DM, the impedance matching and bandwidth of the center slot depend on the width of slot, i.e., d and the width of PIFA, i.e., W_p, while that of the fringe radiated magnetic currents depend on the size of the ground plane, i.e., W_g and L_g. To quantify the influence, the simulated CM and DM impedance bandwidth with the variation of d, W_p, W_g, and L_g is demonstrated in Fig. 11. As shown in Fig. 11(a), with the increasing of the center slot width d, the radiation capacity of DM can be significantly enhanced with an increased impedance bandwidth while the bandwidth of CM almost keeps unchanged. As shown in Fig. 11(b), with the increasing of the width of PIFA W_p, the bandwidth of DM can also be significantly enhanced due to the radiation enhancement of the center slot while the bandwidth of CM almost keeps unchanged. As shown in Fig. 11(c), the bandwidth of DM is enhanced with the shrunk of the width of the ground plane W_g because the radiation capacity of the fringe magnetic currents can be enhanced with a weakened surface-wave effect on a small ground plane. Also, the bandwidth of CM almost keeps unchanged with the shrunk of W_g. As shown in Fig. 11(d), with the shrunk of the length of the ground plane L_g, the bandwidth of CM is decreased while that of DM is enhanced, thus it is an effective degree of freedom to match the bandwidth of CM and DM.

Based on the above analysis, in addition to the intrinsic parameters and the element distance of PIFAs, the size of the ground plane is also a significant factor to match CM and DM impedances, hence we can tune CM and DM impedances to the same state with a self-decoupled performance by simply adjusting the size of the ground plane. As illustrated in Fig. 12, there are also two steps to fulfill coupling reduction for the strongly coupled PIFAs.

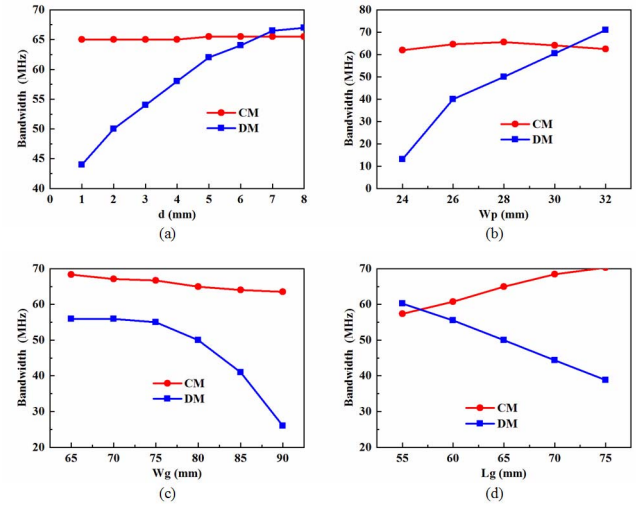

Fig. 11. Simulated CM and DM impedance bandwidth with the variation of (a) side-by-side distance d, (b) width of PIFA W_p, (c) width of the ground plane W_g, and (d) length of the ground plane L_g.

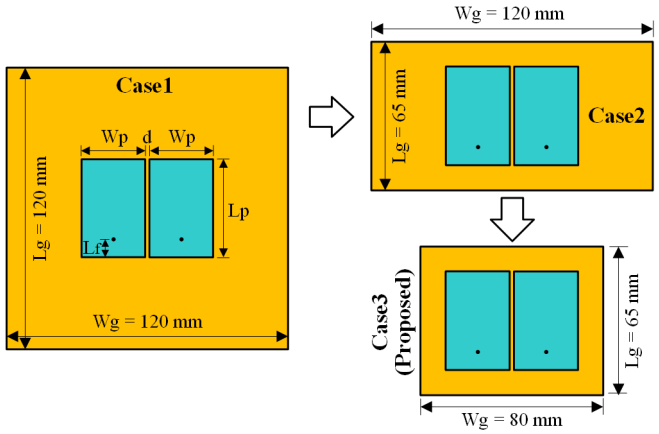

Fig. 12. Evolution procedure of the PIFA decoupling. Only the dimension of the ground plane is altered in the decoupling process. Detailed dimensions: $L_p = 43$ mm, $W_p = 28$ mm, $d = 2$ mm, $L_f = 8$ mm, and $H_p = 8$ mm.

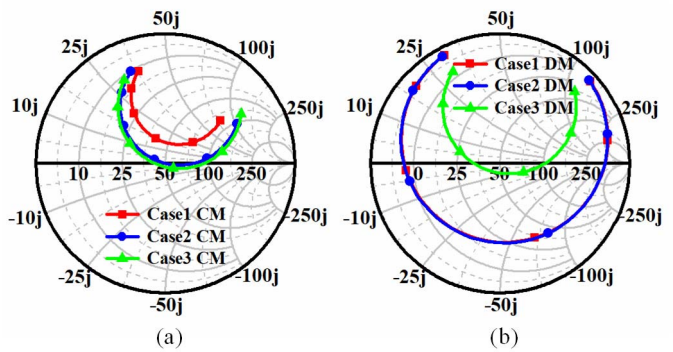

Fig. 13. Smith chart of (a) CM and (b) DM impedances.

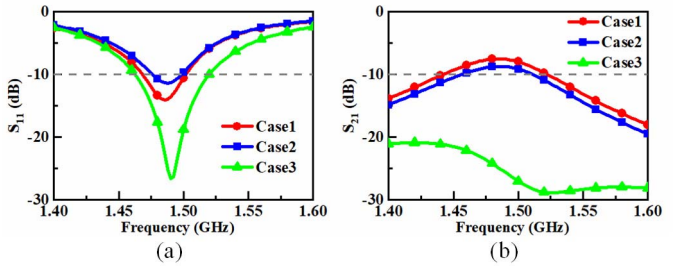

Fig. 14. Simulated (a) S_{11} and (b) S_{21} in the evolution process.

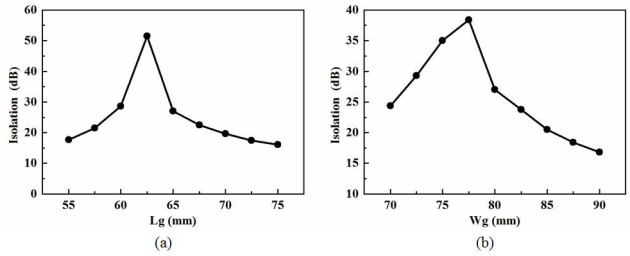

Fig. 15. Simulated isolation at 1.5 GHz with the variation of (a) length of the ground plane L_g (when $W_g = 80$ mm) and (b) width of the ground plane W_g (when $L_g = 65$ mm).

Step 1: Reduce the length L_g of the ground plane as shown in Case2 of Fig. 12. With the shrunk of L_g, the CM impedance can be adjusted independently and tuned to a matched status while the DM impedance almost remains unchanged, as shown in Fig. 13 (blue line).

Step 2: Reduce the width W_g of the ground plane as shown in Case3 of Fig. 12. With the shrunk of W_g, the DM impedance can be adjusted independently and tuned to a matched status while the CM impedance remains unchanged, as shown in Fig. 13 (green line).

B. Decoupling Performance

With the same impedance status for CM and DM, the strong coupling between two closely spaced PIFAs can be canceled out according to (5). The single-ended S-parameters in the evolution procedure are presented in Fig. 14. As seen, the original isolation between two PIFAs is only 7.5 dB when the ground plane dimension is 120×120 mm^2. However, the mutual coupling can be absolutely eliminated and the isolation between two PIFAs can be improved to better than 22.2 dB if the ground plane is shrunk to 65×80 mm^2, without adding any extra decoupling structure. Meanwhile, the matched bandwidth is also enhanced to 1.46~1.52 GHz with the reduction of the ground plane dimension. That is, a novel self-decoupling phenomenon is realized between two extremely closely spaced PIFAs by simply modifying the size of the ground plane.

To further demonstrate the effect of the ground plane size on the element isolation, the simulated isolation at 1.5 GHz with the variation of L_g and W_g is proposed in Fig. 15. As shown in Fig. 15(a), the isolation at 1.5 GHz has an optimal value of 51.5 dB when $L_g = 62.5$ mm. The isolation will be deteriorated with a smaller or larger length L_g of the ground plane. Note that the final dimension of L_g is chosen to 65 mm to balance the radiation pattern and manufacturability. As shown in Fig. 15(b), the isolation at 1.5 GHz also has an

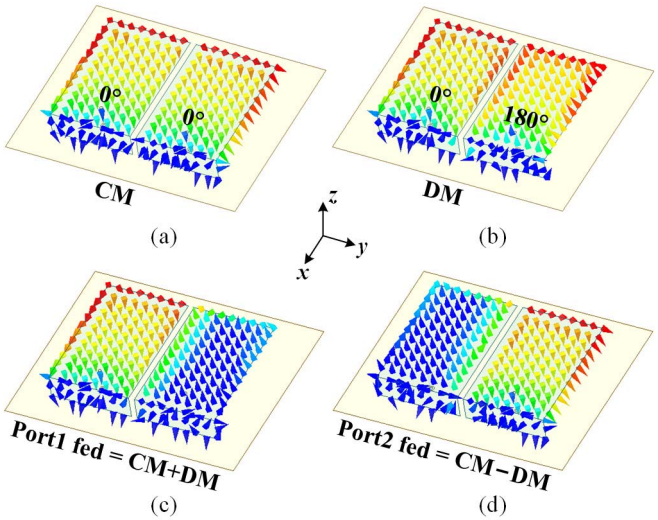

Fig. 16. Vector E-field distributions for the decoupled PIFAs with (a) CM excitation, (b) DM excitation, (c) port1 excitation, and (d) port2 excitation.

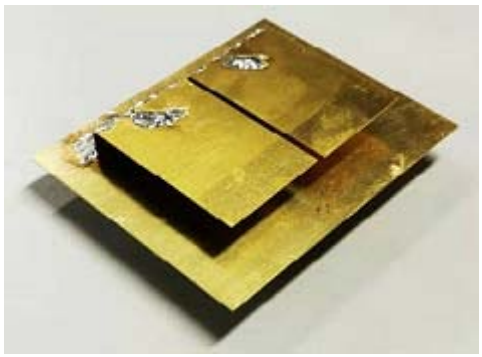

Fig. 17. Photograph of the self-decoupled PIFAs.

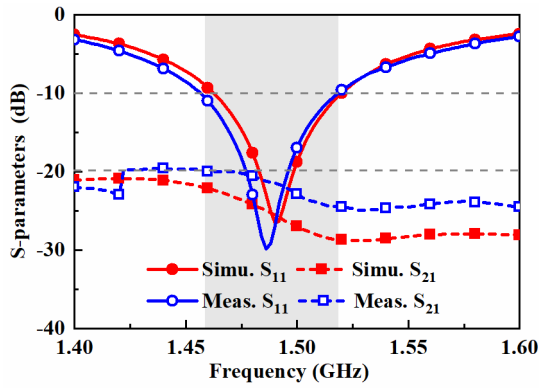

Fig. 18. Simulated and measured S-parameters of the self-decoupled PIFAs.

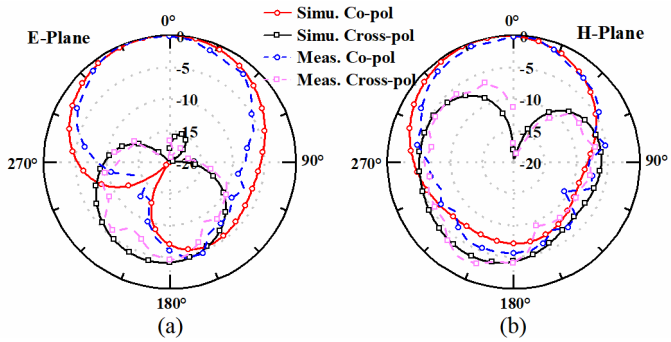

Fig. 19. Simulated and measured normalized radiation pattern of the self-decoupled PIFAs at 1.5 GHz when fed through port1. (a) E-plane. (b) H-plane.

optimal value of 38.4 dB when $W_g = 77.5$ mm. Note that the final result of W_g is chosen to 80 mm to balance the radiation pattern and manufacturability.

The vector E-field distributions for the proposed decoupled PIFAs are illustrated in Fig. 16. Fig. 16(a) and (b) shows the CM and DM E-fields with in-phase and out-of-phase excitations, respectively. Although the E-field distributions in Fig. 16(a) and (b) are similar to those in Fig. 10(b) and (c), however, the E-field strengths of CM and DM are changed to the same with each other. As early analyzed in Section II-B and Fig. 2, the single-ended field distribution can be regarded as the superposition of CM and DM fields. When CM and DM E-fields possess equal strength, the E-field in the passive PIFA can be completely canceled out as shown in Fig. 16(c) and (d).

C. Measured Results

To demonstrate the performance of the proposed self-decoupling PIFAs, a prototype was fabricated as shown in Fig. 17. The prototype is manufactured by 0.3 mm thick brass ($\sigma = 1.5\times10^7$ S/m) plates with the laser cutting process. Two copper pillars are soldered with the PIFAs as the feeding probes. And two 50 Ω SMA connectors are employed beneath the ground plane for antenna test.

The measured S-parameter is plotted in Fig. 18, showing a good agreement with the simulated results. Both simulated and measured results demonstrate a −10 dB S_{11} bandwidth of 1.46–1.52 GHz (4.0%). Across the matched bandwidth, a high measured isolation of better than 20.0 dB is realized.

The simulated and measured E-plane and H-plane normalized radiation patterns when fed through port1 are presented in Fig. 19(a) and (b), respectively. The radiation pattern fed through port2 is symmetrical to that of port1, which is not shown for brevity. As seen, a directional radiation pattern with a low cross-polarization in the broadside direction is realized in both planes. However, the backward radiation is increased because of the reduction of the ground plane.

The simulated and measured total efficiency is shown in Fig. 20. Across the desired band, the simulated efficiency is 84.0%−99.9%, while the measured one is 86.4%−95.9%. The ultralow loss of air medium and the good impedance matching and isolation performance contributes to the proposed high antenna efficiency.

To evaluate the diversity performance of the proposed self-decoupled PIFAs, the simulated and measured envelope correlation coefficients (ECCs) are presented in Fig. 20. The ECCs are deduced by the simulated and measured far E-fields

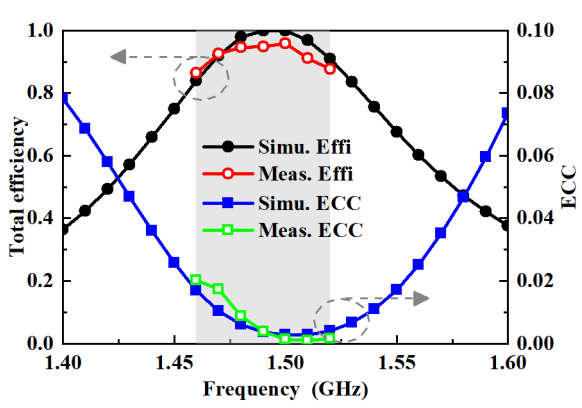

Fig. 20. Simulated and measured total efficiency and ECC of the self-decoupled PIFAs.

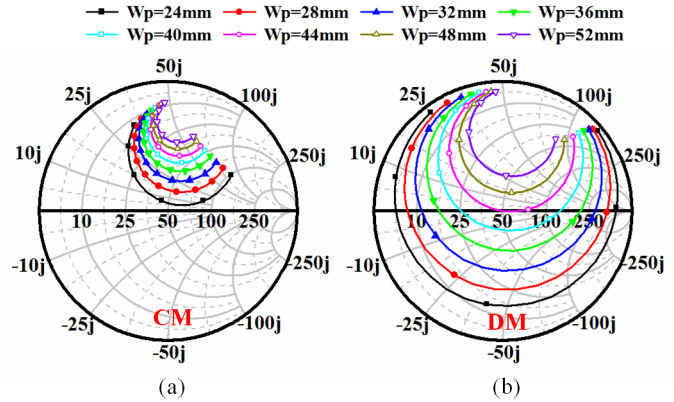

Fig. 21. Simulated (a) CM and (b) DM impedances with the variation of W_p under a large ground plane (120 × 120 mm^2).

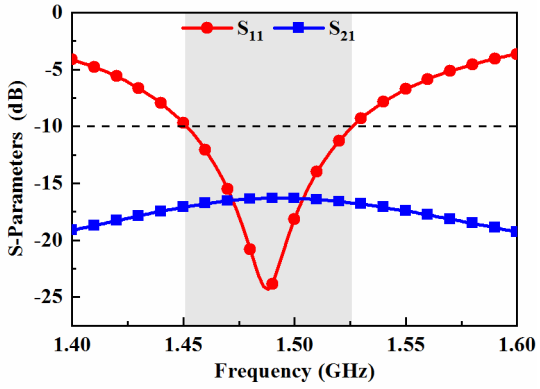

Fig. 22. Simulated S-parameters with an increased W_p for self-decoupling under a large ground plane. Detailed dimensions: L_g = 120 mm, W_g = 120 mm, L_p = 43 mm, W_p = 52 mm, d = 2 mm, L_f = 13 mm, H_p = 8 mm.

TABLE III
COMPARISON OF THE DECOUPLING PERFORMANCE BETWEEN CLOSELY SPACED PIFAS

Ref	Decoupling structure	Distance	-10 dB S_{11} Bandwidth	Isolation
[21]	DGS	0.015 λ_0	3.0%	> 20dB
[22]	DGS	0.02 λ_0	4.1%	> 20dB
[25]	NL	0.12 λ_0	6.4%	> 18dB
[26]	NL	0.03 λ_0	3.8%	> 9dB
Proposed1*	×	0.01 λ_0	4.0%	> 22.2dB
Proposed2**	×	0.01 λ_0	5.0%	> 16.3 dB

* Proposed1 is decoupled by the modification of the size of the ground plane.
** Proposed2 is decoupled by the modification of the width W_g of PIFA.

based on the formulation [48]

$$\rho_e \approx |\rho_c|^2 = \left| \frac{\oiint A_{12}(\theta,\varphi)\sin\theta \mathrm{d}\theta\mathrm{d}\varphi}{\oiint A_{11}(\theta,\varphi)\sin\theta \mathrm{d}\theta\mathrm{d}\varphi \cdot \oiint A_{22}(\theta,\varphi)\sin\theta \mathrm{d}\theta\mathrm{d}\varphi} \right|^2 \quad (9)$$

where

$$A_{ij} = E_{\theta,i}(\theta,\varphi)\cdot E^*_{\theta,j}(\theta,\varphi) + E_{\varphi,i}(\theta,\varphi)\cdot E^*_{\varphi,j}(\theta,\varphi). \quad (10)$$

Here, $E_{\theta,i}$ and $E_{\varphi,i}$ are the complex electric field of port i in the elevation and azimuth planes, respectively. As shown in Fig. 20, both simulated and measured results demonstrate a good diversity performance for the proposed self-decoupled PIFAs with ECCs < 0.02 across the desired band.

D. Other Decoupling Scheme

It should be noted that the proposed self-decoupling design scheme with a modified ground plane size is not suitable for the application when the size of the ground plane is strictly fixed, such as mobile phone antennas. Therefore, to fit different application scenarios, other parameter to tune CM and DM impedances, within a fixed ground plane of 120 × 120 mm^2, is also proposed. As analyzed in Section IV-A, the width W_p of PIFA shows a significant impact on the impedance bandwidth of DM. Fig. 21 shows the simulated CM and DM impedances with the variation of W_p under a ground plane of 120 × 120 mm^2. As seen, with the increasing of W_p, both of the CM and DM impedances shift upward to the inductive region, but the variation of DM impedance is severer than CM impedance. Thus, the discrepancy between CM and DM impedances can be reduced by increasing W_p. When W_p is increased to 52 mm, the simulated S-parameters are presented in Fig. 22 (note that the feed position is optimized to L_f = 13 mm for a good impedance matching). As seen, a good self-decoupling performance with an isolation better than 16.3 dB and an operating bandwidth of 5.0% is also realized.

E. Comparison

To highlight the advantages of the proposed PIFA decoupling scheme, it is compared to the conventional decoupling techniques for closely spaced PIFAs as listed in Table III. The conventional decoupling techniques for closely spaced PIFAs are DGS [21], [22] and NLs [25], [26]. The DGS technique can achieve acceptable decoupling performance for closely spaced PIFAs; however, the radiation pattern will be affected by the resonant slot on the ground plane with a strong backward leakage. The NL technique can realize a

good isolation performance when two PIFAs are separated by some distance, but the decoupling performance is significantly degraded when the interdistance of two PIFAs is reduced to 0.03 λ_0 [26]. Consequently, compared to the above-mentioned PIFA decoupling techniques, our proposed decoupling scheme possesses the merits of self-decoupling (without extra decoupling structure), extremely closely spaced element distance (0.01 λ_0), moderate bandwidth, and good isolation performance, which is a potential candidate for MIMO applications.

V. Conclusion

This article proposes a simple and efficient decoupling method based on a new perspective of CM and DM cancellation. In our method, the complex decoupling problem can be transformed to the CM and DM impedance matching, which provides a simplified perspective on antenna decoupling. Moreover, with the help of unique orthogonal field properties of CM and DM, the CM and DM impedances can be adjusted independently to avoid the complex iteration process.

Two classic design examples, including the decoupling between closely spaced dipoles and PIFAs, are proposed to demonstrate the novelty of this method. For dipole antennas, by inserting two horizontal strips for DM impedance matching and a capacitance-loaded vertical strip for CM impedance matching, the strong mutual coupling between two dipoles can be suppressed with a superb bandwidth performance. For PIFAs, by adjusting the size of the ground plane or the width of PIFAs, the strong mutual coupling between two extremely closely spaced PIFAs can be self-decoupled without using any extra decoupling structure. Both design examples have verified that the proposed decoupling method possesses systemic design guideline, simplified decoupling procedure, and satisfactory decoupling performance. We further envision that this decoupling methodology could be applied in various antenna types to solve the intricate coupling problem in a systemic and intuitive way.

References

[1] M. A. Jensen and J. W. Wallace, "A review of antennas and propagation for MIMO wireless communications," *IEEE Trans. Antennas Propag.*, vol. 52, no. 11, pp. 2810–2824, Nov. 2004.

[2] X. Chen, S. Zhang, and Q. Li, "A review of mutual coupling in MIMO systems," *IEEE Access*, vol. 6, pp. 24706–24719, 2018.

[3] H. Li and B. K. Lau, "MIMO systems and antennas for terminals," in *Handbook of Antenna Technologies*, Z. N. Chen, D. Liu, H. Nakano, X. Qing, and T. Zwick, Eds. Singapore: Springer, 2016.

[4] S.-C. Chen, Y.-S. Wang, and S.-J. Chung, "A decoupling technique for increasing the port isolation between two strongly coupled antennas," *IEEE Trans. Antennas Propag.*, vol. 56, no. 12, pp. 3650–3658, Dec. 2008.

[5] Y. Li, Z. Zhang, W. Chen, Z. Feng, and M. F. Iskander, "A dual-polarization slot antenna using a compact CPW feeding structure," *IEEE Antennas Wireless Propag. Lett.*, vol. 9, pp. 191–194, 2010.

[6] Y. Li, Z. Zhang, J. Zheng, and Z. Feng, "Compact azimuthal omnidirectional dual-polarized antenna using highly isolated colocated slots," *IEEE Trans. Antennas Propag.*, vol. 60, no. 9, pp. 4037–4045, Sep. 2012.

[7] C. Deng, Y. Li, Z. Zhang, and Z. Feng, "A wideband high-isolated dual-polarized patch antenna using two different balun feedings," *IEEE Antennas Wireless Propag. Lett.*, vol. 13, pp. 1617–1619, 2014.

[8] L. Sun, H. Feng, Y. Li, and Z. Zhang, "Compact 5G MIMO mobile phone antennas with tightly arranged orthogonal-mode pairs," *IEEE Trans. Antennas Propag.*, vol. 66, no. 11, pp. 6364–6369, Nov. 2018.

[9] L. Chang, Y. Yu, K. Wei, and H. Wang, "Polarization-orthogonal co-frequency dual antenna pair suitable for 5G MIMO smartphone with metallic bezels," *IEEE Trans. Antennas Propag.*, vol. 67, no. 8, pp. 5212–5220, Aug. 2019.

[10] L. Sun, Y. Li, Z. Zhang, and Z. Feng, "Wideband 5G MIMO antenna with integrated orthogonal-mode dual-antenna pairs for metal-rimmed smartphones," *IEEE Trans. Antennas Propag.*, vol. 68, no. 4, pp. 2494–2503, Apr. 2020.

[11] K. Wei, Z. Zhang, W. Chen, and Z. Feng, "A novel hybrid-fed patch antenna with pattern diversity," *IEEE Antennas Wireless Propag. Lett.*, vol. 9, pp. 562–565, 2010.

[12] C. Deng, X. Lv, and Z. Feng, "Wideband dual-mode patch antenna with compact CPW feeding network for pattern diversity application," *IEEE Trans. Antennas Propag.*, vol. 66, no. 5, pp. 2628–2633, May 2018.

[13] L. Sun, Y. Li, Z. Zhang, and M. F. Iskander, "A compact planar omnidirectional MIMO array antenna with pattern phase diversity using folded dipole element," *IEEE Trans. Antennas Propag.*, vol. 67, no. 3, pp. 1688–1696, Mar. 2019.

[14] L. Sun, Y. Li, Z. Zhang, and Z. Feng, "Compact co-horizontally polarized full-duplex antenna with omnidirectional patterns," *IEEE Antennas Wireless Propag. Lett.*, vol. 18, no. 6, pp. 1154–1158, Jun. 2019.

[15] F. Yang and Y. Rahmat-Samii, "Microstrip antennas integrated with electromagnetic band-gap (EBG) structures: A low mutual coupling design for array applications," *IEEE Trans. Antennas Propag.*, vol. 51, no. 10, pp. 2936–2946, Oct. 2003.

[16] E. Rajo-Iglesias, Ó. Quevedo-Teruel, and L. Inclan-Sanchez, "Mutual coupling reduction in patch antenna arrays by using a planar EBG structure and a multilayer dielectric substrate," *IEEE Trans. Antennas Propag.*, vol. 56, no. 6, pp. 1648–1655, Jun. 2008.

[17] H. S. Farahani, M. Veysi, M. Kamyab, and A. Tadjalli, "Mutual coupling reduction in patch antenna arrays using a UC-EBG superstrate," *IEEE Antennas Wireless Propag. Lett.*, vol. 9, pp. 57–59, 2010.

[18] C.-Y. Chiu, C.-H. Cheng, R. D. Murch, and C. R. Rowell, "Reduction of mutual coupling between closely-packed antenna elements," *IEEE Trans. Antennas Propag.*, vol. 55, no. 6, pp. 1732–1738, Jun. 2007.

[19] A. Habashi, J. Nourinia, and C. Ghobadi, "Mutual coupling reduction between very closely spaced patch antennas using low-profile Folded Split-Ring Resonators (FSRRs)," *IEEE Antennas and Wireless Propag. Lett.*, vol. 10, pp. 862–865, 2011.

[20] S. Zhang, J. Xiong, and S. He, "MIMO antenna system of two closely-positioned PIFAs with high isolation," *Electron. Lett.*, vol. 45, no. 15, pp. 771–773, Jul. 2009.

[21] S. Zhang, S. N. Khan, and S. He, "Reducing mutual coupling for an extremely closely-packed tunable dual-element PIFA array through a resonant slot antenna formed in-between," *IEEE Trans. Antennas Propag.*, vol. 58, no. 8, pp. 2771–2776, Aug. 2010.

[22] S. Zhang, B. K. Lau, Y. Tan, Z. Ying, and S. He, "Mutual coupling reduction of two PIFAs with a T-Shape slot impedance transformer for MIMO mobile terminals," *IEEE Trans. Antennas Propag.*, vol. 60, no. 3, pp. 1521–1531, Mar. 2012.

[23] J. OuYang, F. Yang, and Z. M. Wang, "Reducing mutual coupling of closely spaced microstrip MIMO antennas for WLAN application," *IEEE Antennas Wireless Propag. Lett.*, vol. 10, pp. 310–313, 2011.

[24] A. Diallo, C. Luxey, P. L. Thuc, R. Staraj, and G. Kossiavas, "Study and reduction of the mutual coupling between two mobile phone PIFAs operating in the DCS1800 and UMTS bands," *IEEE Trans. Antennas Propag.*, vol. 54, no. 11, pp. 3063–3074, Nov. 2006.

[25] A. Diallo, C. Luxey, P. L. Thuc, R. Staraj, and G. Kossiavas, "Enhanced two-antenna structures for universal mobile telecommunications system diversity terminals," *IET Microw., Antennas Propag.*, vol. 2, no. 1, pp. 93–101, Feb. 2008.

[26] A. Chebihi, C. Luxey, A. Diallo, P. Le Thuc, and R. Staraj, "A novel isolation technique for closely spaced PIFAs for UMTS mobile phones," *IEEE Antennas Wireless Propag. Lett.*, vol. 7, pp. 665–668, 2008.

[27] Y. Wang and Z. Du, "A wideband printed dual-antenna system with a novel neutralization line for mobile terminals," *IEEE Antennas Wireless Propag. Lett.*, vol. 12, pp. 1428–1431, Oct. 2013.
[28] Y. Wang and Z. Du, "A wideband printed dual-antenna with three neutralization lines for mobile terminals," *IEEE Trans. Antennas Propag.*, vol. 62, no. 3, pp. 1495–1500, Mar. 2014.
[29] A. C. K. Mak, C. R. Rowell, and R. D. Murch, "Isolation enhancement between two closely packed antennas," *IEEE Trans. Antennas Propag.*, vol. 56, no. 11, pp. 3411–3419, Nov. 2008.
[30] B. K. Lau and J. B. Andersen, "Simple and efficient decoupling of compact arrays with parasitic scatters," *IEEE Trans. Antennas Propag.*, vol. 60, no. 2, pp. 464–472, Feb. 2012.
[31] S. Farsi, H. Aliakbarian, D. Schreurs, B. Nauwelaers, and G. A. E. Vandenbosch, "Mutual coupling reduction between planar antennas by using a simple microstrip U-Section," *IEEE Antennas Wireless Propag. Lett.*, vol. 11, pp. 1501–1503, 2012.
[32] L. Zhao and K.-L. Wu, "A decoupling technique for four-element symmetric arrays with reactively loaded dummy elements," *IEEE Trans. Antennas Propag.*, vol. 62, no. 8, pp. 4416–4421, Aug. 2014.
[33] S. Hong, K. Chung, J. Lee, S. Jung, S.-S. Lee, and J. Choi, "Design of a diversity antenna with stubs for UWB applications," *Microw. Opt. Technol. Lett.*, vol. 50, no. 5, pp. 1352–1356, 2008.
[34] H. Wang, L. Liu, Z. Zhang, Y. Li, and Z. Feng, "A wideband compact WLAN/WiMAX MIMO antenna based on dipole with V-shaped ground branch," *IEEE Trans. Antennas Propag.*, vol. 63, no. 5, pp. 2290–2295, May 2015.
[35] H. Qi, L. Liu, X. Yin, H. Zhao, and W. J. Kulesza, "Mutual coupling suppression between two closely spaced microstrip antennas with an asymmetrical coplanar strip wall," *IEEE Antennas Wireless Propag. Lett.*, vol. 15, pp. 191–194, 2016.
[36] Z. Ren, A. Zhao, and S. Wu, "MIMO antenna with compact decoupled antenna pairs for 5G mobile terminals," *IEEE Antennas Wireless Propag. Lett.*, vol. 18, no. 7, pp. 1367–1371, Jul. 2019.
[37] J. Sui and K.-L. Wu, "Self-curing decoupling technique for two Inverted-F antennas with capacitive loads," *IEEE Trans. Antennas Propag.*, vol. 66, no. 3, pp. 1093–1101, Mar. 2018.
[38] K.-L. Wu, C. Wei, X. Mei, and Z.-Y. Zhang, "Array-antenna decoupling surface," *IEEE Trans. Antennas Propag.*, vol. 65, no. 12, pp. 6728–6738, Dec. 2017.
[39] M. Li, B. G. Zhong, and S. W. Cheung, "Isolation enhancement for MIMO patch antennas using near-field resonators as coupling-mode transducers," *IEEE Trans. Antennas Propag.*, vol. 67, no. 2, pp. 755–764, Feb. 2019.
[40] J. Guo, F. Liu, L. Zhao, Y. Yin, G.-. L. Huang, and Y. Li, "Meta-surface antenna array decoupling designs for two linear polarized antennas coupled in H-plane and E-plane," *IEEE Access*, vol. 7, pp. 100442–100452, Jul. 2019.
[41] Z. Niu, H. Zhang, Q. Chen, and T. Zhong, "Isolation enhancement in closely coupled dual-band MIMO patch antennas," *IEEE Antennas Wireless Propag. Lett.*, vol. 18, no. 8, pp. 1686–1690, Aug. 2019.
[42] L. Sun, G.-X. Zhang, B.-H. Sun, W.-D. Tang, and J.-P. Yuan, "A single patch antenna with broadside and conical radiation patterns for 3G/4G pattern diversity," *IEEE Antennas Wireless Propag. Lett.*, vol. 15, pp. 433–436, 2016.
[43] X. Jiang, Z. Zhang, Y. Li, and Z. Feng, "A novel null scanning antenna using even and odd modes of a shorted patch," *IEEE Trans. Antennas Propag.*, vol. 62, no. 4, pp. 1903–1909, Apr. 2014.
[44] Z. Xu and C. Deng, "High-isolated MIMO antenna design based on pattern diversity for 5G mobile terminals," *IEEE Antennas Wireless Propag. Lett.*, vol. 19, no. 3, pp. 467–471, Mar. 2020.
[45] L. Sun, Y. Li, Z. Zhang, and H. Wang, "Self-decoupled MIMO antenna pair with shared radiator for 5G smartphones," *IEEE Trans. Antennas Propag.*, vol. 68, no. 5, pp. 3423–3432, May 2020.
[46] D. E. Bockelman and W. R. Eisenstadt, "Combined differential and common-mode scattering parameters: Theory and simulation," *IEEE Trans. Microw. Theory Techn.*, vol. 43, no. 7, pp. 1530–1539, Jul. 1995.
[47] M.-C. Huynh and W. Stutzman, "Ground plane effects on planar inverted-F antenna (PIFA) performance," *IEE Proc.-Microw., Antennas Propag.*, vol. 150, no. 4, pp. 209–213, Aug. 2003.
[48] R. G. Vaughan and J. B. Andersen, "Antenna diversity in mobile communications," *IEEE Trans. Veh. Technol.*, vol. VT-36, no. 4, pp. 147–172, Nov. 1987.

Libin Sun (Graduate Student Member, IEEE) received the B.S. degree from Xidian University, Xi'an, China, in 2016. He is currently pursuing the Ph.D. degree with the Department of Electrical and Engineering, Tsinghua University, Beijing, China.

He has authored over ten journal papers, and holds five granted Chinese patents. His current research interest includes antenna design and theory, particularly in 5G mobile phone antennas, multi-input multi-output (MIMO) and diversity antennas, circularly polarized antennas, leaky-wave antennas, and surface-wave antennas.

Mr. Sun was a recipient of the Outstanding Reviewer for the IEEE TRANSACTIONS ON ANTENNAS AND PROPAGATION in 2019 and the Honorable Mention in the 2020 IEEE AP-S Student Paper Competition. He serves as a Reviewer for several international academic journals, such as the IEEE TRANSACTIONS ON ANTENNAS AND PROPAGATION, the IEEE ANTENNAS AND WIRELESS PROPAGATION LETTERS, IEEE ACCESS, the *IET Microwaves, Antennas & Propagation*, the *IET Electronics Letters*, and *Microwave and Optical Technology Letters*.

Yue Li (Senior Member, IEEE) received the B.S. degree in telecommunication engineering from Zhejiang University, Zhejiang, China, in 2007, and the Ph.D. degree in electronic engineering from Tsinghua University, Beijing, China, in 2012.

In June 2012, he was a Post-Doctoral Fellow with the Department of Electronic Engineering, Tsinghua University. In December 2013, he was a Research Scholar with the Department of Electrical and Systems Engineering, University of Pennsylvania, Philadelphia, PA, USA. He was also a Visiting Scholar with the Institute for Infocomm Research (I2R), A∗STAR, Singapore, in 2010, and the Hawaii Center of Advanced Communication (HCAC), University of Hawaii at Manoa, Honolulu, HI, USA, in 2012. Since January 2016, he has been with Tsinghua University, where he is currently an Assistant Professor. He is currently an Associate Professor with the Department of Electronic Engineering, Tsinghua University. He has authored or coauthored over 130 journal papers and 45 international conference papers, and holds 18 granted Chinese patents. His current research interests include metamaterials, plasmonics, electromagnetics, nanocircuits, mobile and handset antennas, multi-input multi-output (MIMO) and diversity antennas, and millimeter-wave antennas and arrays.

Dr. Li was a recipient of the Issac Koga Gold Medal from the URSI General Assembly in 2017; the Second Prize of the Science and Technology Award of the China Institute of Communications in 2017; the Young Scientist Awards from the conferences of ACES 2018, AT-RASC 2018, AP-RASC 2016, EMTS 2016, and URSI GASS 2014; the Best Paper Awards from the conferences of CSQRWC 2018, NCMMW 2018 and 2017, APCAP 2017, NCANT 2017, ISAPE 2016, and ICMMT 2016; the Outstanding Doctoral Dissertation of Beijing Municipality in 2013; and the Principal Scholarship of Tsinghua University in 2011. He is serving as an Associate Editor for the IEEE TRANSACTIONS ON ANTENNAS AND PROPAGATION, the IEEE ANTENNAS AND WIRELESS PROPAGATION LETTERS, and *Computer Applications in Engineering Education*, and also on the Editorial Board of *Scientific Reports*.

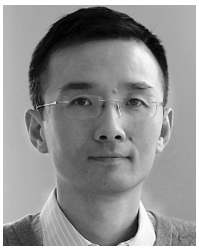

Zhijun Zhang (Fellow, IEEE) received the B.S. and M.S. degrees from the University of Electronic Science and Technology of China, Chengdu, China, in 1992 and 1995, respectively, and the Ph.D. degree from Tsinghua University, Beijing, China, in 1999.

In 1999, he was a Post-Doctoral Fellow with the Department of Electrical Engineering, The University of Utah, Salt Lake City, UT, USA, where he was appointed a Research Assistant Professor in 2001. In May 2002, he was an Assistant Researcher with the University of Hawaii at Manoa, Honolulu, HI, USA. In November 2002, he joined Amphenol T&M Antennas, Vernon Hills, IL, USA, as a Senior Staff Antenna Development Engineer, and was then promoted to the position of an Antenna Engineer Manager. In 2004, he joined Nokia Inc., San Diego, CA, as a Senior Antenna Design Engineer. In 2006, he joined Apple Inc., Cupertino, CA, USA, as a Senior Antenna Design Engineer and was then promoted to the position of a Principal Antenna Engineer. Since August 2007, he has been with Tsinghua University, where he is currently a Professor with the Department of Electronic Engineering. He is the Author of the book *Antenna Design for Mobile Devices* (Wiley, First Edition in 2011 and Second Edition in 2017).

Dr. Zhang served as an Associate Editor for the IEEE TRANSACTIONS ON ANTENNAS AND PROPAGATION from 2010 to 2014 and the IEEE ANTENNAS AND WIRELESS PROPAGATION LETTERS from 2009 to 2015.

Hanyang Wang (Senior Member, IEEE) received the Ph.D. degree from Heriot-Watt University, Edinburgh, U.K., in 1995.

From 1986 to 1991, he served as a Lecturer and an Associate Professor with Shandong University, Jinan, China. From 1995 to 1999, he was a Post-Doctoral Research Fellow with the University of Birmingham, Birmingham, U.K., and the University of Essex, Colchester, U.K. From 1999 to 2000, he was with Vector Fields Ltd., Oxford, U.K., as a Software Development and Microwave and Antenna Engineering Consultant Engineer. He joined Nokia U.K. Ltd., Farnborough, U.K., in 2001, where he had been a Mobile Antenna Specialist for 11 years. He joined Huawei Technology Ltd., Berkshire, U.K., after leaving Nokia, where he is currently the Chief Mobile Antenna Expert and the Head of the Mobile Antenna Technology Division. He is also an Adjunct Professor with Nanjing University, Nanjing, China, and Sichuan University, Chengdu, China. He holds over 40 granted U.S./European/Japan/Chinese patents. His current research interests include small, wideband and multiband antennas for mobile terminals, antennas, and antenna arrays for 5G mobile communications in sub-6 GHz and mm-wave frequency bands. He has authored over 100 articles on these topics.

Dr. Wang is a Huawei Fellow and an IET Fellow. He was a recipient of the Title of Nokia Inventor of the Year in 2005, the Nokia Excellence Award in 2011, the Huawei Individual Gold Medal Award in 2012, and the Huawei Team Gold Medal Award in 2013 and 2014. His patent was ranked number one among 2015 Huawei top ten patent awards. He is an Associate Editor of the IEEE ANTENNAS AND WIRELESS PROPAGATION LETTERS.